Amplification of the linear and nonlinear optical response of a chiral molecular crystal

Domingos, S.R.; Pereira Silva, P.S.; Buma, W.J.; Garcia, M.H.; Lopes, N.C.; Paixao, J.A.; Silva, M.R.; Woutersen, S.

DOI
10.1063/1.3697842

Publication date
2012

Document Version
Final published version

Published in
Journal of Chemical Physics

Amplification of the linear and nonlinear optical response of a chiral molecular crystal

Sérgio R. Domingos, Pedro S. Pereira Silva, Wybren Jan Buma, M. Helena Garcia, Nelson C. Lopes et al.

Citation: J. Chem. Phys. **136**, 134501 (2012); doi: 10.1063/1.3697842
View online: http://dx.doi.org/10.1063/1.3697842
View Table of Contents: http://jcp.aip.org/resource/1/JCPSA6/v136/i13
Published by the American Institute of Physics.

Amplification of the linear and nonlinear optical response of a chiral molecular crystal

Sérgio R. Domingos,[1,a)] Pedro S. Pereira Silva,[2,b)] Wybren Jan Buma,[1] M. Helena Garcia,[3] Nelson C. Lopes,[4] José António Paixão,[2] Manuela Ramos Silva,[2] and Sander Woutersen[1]
[1]*Van't Hoff Institute for Molecular Sciences, University of Amsterdam, Science Park 904, 1098 XH Amsterdam, The Netherlands*
[2]*CEMDRX, Physics Department, University of Coimbra, P-3004-516 Coimbra, Portugal*
[3]*Faculdade de Ciências da Universidade de Lisboa, Ed. C8 Campo Grande, P-1749-016 Lisbon, Portugal*
[4]*GoLP/Centro de Física dos Plasmas, Instituto Superior Técnico, P-1049-001 Lisbon, Portugal*

(Received 26 December 2011; accepted 3 March 2012; published online 2 April 2012)

We have observed large second-order nonlinear optical and vibrational circular dichroism (VCD) responses in a charge-transfer-type L-Histidinium salt. Using X-ray Diffraction, VCD spectroscopy, and time-dependent density functional theory to characterize the compound, we employ a two-level model to explain and quantify the strongly enhanced optical signals. We find that both linear and nonlinear optical responses are greatly enhanced by a single low-lying charge-transfer state. © *2012 American Institute of Physics*. [http://dx.doi.org/10.1063/1.3697842]

I. INTRODUCTION

The majority of the early nonlinear optical materials were inorganic crystals. In the last three decades, focus has shifted toward organic compounds due to the much larger design flexibility they offer, which allows for a fine tuning of the microscopic properties and thus of the linear and nonlinear optical susceptibilities.[1,2] Organic materials have been found to exhibit second-harmonic generation (SHG) efficiencies that by far exceed those of inorganic nonlinear optical (NLO) crystals such as lithium niobate ($LiNbO_3$) or potassium dihydrogen phosphate (KDP).[3,4] Other advantages of organic materials include fast response times and high optical damage thresholds. Apart from the more common push-pull molecules, several approaches to chromophore optimization have been proposed such as the use of octupolar systems[5,6] and molecules with tuned bond length alternation.[7] All these attempts to obtain NLO materials with an enhanced performance lead to molecular systems with the same basic electronic characteristics: a conjugated π-electron system, asymmetrically substituted by electron donor and acceptor groups to ensure the presence of low-lying electronically excited states of strong *intra*molecular charge-transfer excitation character.

An alternative approach to obtain a large NLO response is to devise molecular systems in which charge transfer occurs between non-covalently bound chromophores, i.e., by *inter*molecular or "through-space" charge transfer. Di Bella *et al.* performed a computational study of intermolecular charge transfer for a variety of donor-acceptor pairs.[8] Experimentally, the influence of through-space charge transfer on NLO properties has been investigated recently with alternating stacks of 2-amino-1,3-benzothiazole and ethylcoumarin-3-carboxylate.[9] However, the observed NLO response was modest due to the symmetry of the crystal unit cell. Two important studies of substituted paracyclophane compounds,[10,11] using the collective electron oscillation (CEO) approach,[12] also indicated a significant role of through-space charge transfer in the second-order nonlinear response of these compounds. The crystal engineering strategy of co-crystallizing anionic-cationic moieties has also been used to enhance the quadratic nonlinear optical properties.[13–17] It therefore seems clear that low-lying charge-transfer excited states can play an important role in enhanced NLO responses.

Vibrational circular dichroism (VCD) is a spectroscopic technique that is currently used as a highly sensitive infrared probe for stereoisomer identification, absolute configuration, and conformation assignment. Recent work has shown that modulation of the energies of the excited-state manifold can lead to an order-of-magnitude enhancement of the VCD signals.[18] The enhancement of NLO and VCD signals thus finds a common origin in the dominating role of low-lying electronically excited states.

Here, we present experiments on crystals of a novel compound, L-histidinium 5-nitro-2,4-dioxo-1,2,3,4-tetrahydropyrimidin-1-ide (L-His$^+$5NU$^-$), that confirm this idea. We find that both the NLO (SHG) and VCD response of this crystal are strongly enhanced. We present a quantitative method to predict the magnitude of the enhanced SHG and VCD signals using the same two-level approach that makes use of the ground state and the lowest electronically excited state. We will show that this approach enables quantitative prediction of the observed SHG and VCD signal magnitudes, and thus is a promising method to predict nonlinear and linear responses, thus enabling a systematic approach to optimizing the nonlinear properties of new optical materials.

The paper is organized as follows: in Sec. II we describe the experimental methods used in this work. Section III comprises the theoretical methodologies implemented in the model. In Sec. IV the results (crystal structure, nonlinear susceptibilities, and VCD) are discussed, in particular the

a)Electronic mail: s.m.rosadomingos@uva.nl.
b)Electronic mail: psidonio@pollux.fis.uc.pt.

influence of low-lying electronically excited states on the linear and nonlinear optical response of the crystal. Finally, we show how we can obtain a fairly accurate prediction of the enhanced response using solely the ground and first excited state.

II. EXPERIMENTAL METHODS

A. Synthesis

L-His$^+$5NU$^-$ was prepared by adding 5-nitrouracil (Sigma-Aldrich, 98%, 1 mmol) to L-histidine (Sigma-Aldrich, 97%, 1 mmol) in aqueous solution (100 ml). The solution was slowly warmed and then left to evaporate under ambient conditions. After 2 weeks, small pink transparent single crystals with prismatic habit were deposited.

B. X-ray diffraction studies

1. Single-crystal X-ray

The diffraction measurements for L-His$^+$5NU$^-$ were carried out on a single crystal using Mo Kα radiation on a Bruker APEX II diffractometer.[19] Data reduction was performed with SMART and SAINT software.[19] Lorenz and polarization corrections were applied. Absorption correction was applied using SADABS.[20] The structure was solved by direct methods using the SHELXS-97 program,[21] and refined on F^2s by full-matrix least-squares with the same program.[21] The anisotropic displacement parameters for non-hydrogen atoms were applied. The hydrogen atoms were placed at calculated positions and refined with isotropic parameters as riding atoms. The crystal data and details concerning data collection and structure refinement are given in Table I. Because of the weak anomalous scattering at the Mo Kα wavelength, the absolute structure could not be determined from the X-ray data but was established by the presence of the chiral cation, L-histidinium.

2. Powder X-ray diffraction

The single crystals were powdered thoroughly using a pestle and mortar to prepare a polycrystalline sample. The sample powder was sifted with a 63 μm sieve and a glass capillary of 0.3 mm diameter was filled and used in the data collection. An Enraf-Nonius powder diffractometer equipped with a CPS120 detector and a quartz monochromator selecting the Cu Kα1 wavelength was used for data collection.

C. Kurtz and Perry powder method

The SHG efficiency of L-His$^+$5NU$^-$ was measured using the Kurtz and Perry powder method[22] with an experimental setup that has been described in detail before.[23] The measurements were performed at a wavelength of 1064 nm produced by a Nd:YAG laser operating at 10 Hz and producing 40 ns pulses with a pulse energy of 50 mJ. The sample preparation procedure was as follows: the material was mulled to a fine powder and compacted in a mount and then installed in the sample holder. Sample grain sizes were not standardized. For this reason, signals between individual measurements were seen to vary in some cases by as much as $\pm$20%. For a proper comparison with the urea reference material the measurements were averaged over several laser thermal cycles.

TABLE I. Crystallographic data for L-His$^+$5NU$^-$.

Formula	$C_{10}H_{12}N_6O_6$
Formula weight	312.26
Temperature (K)	293(2)
Wavelength (Å)	0.71073
Crystal system	Monoclinic
Space group	$P2_1$
a (Å)	6.1911(16)
b (Å)	7.332(2)
c (Å)	13.729(4)
α (°)	90
β (°)	99.990(13)
γ (°)	90
Volume (Å^3)	613.8(3)
Z	2
Calc. dens. (g/cm^3)	1.690
Abs. coef. (mm^{-1})	0.142
Reflections (collected/unique)	14 349/1656
R(int)	0.0163
R_1 [$I > 2\sigma(I)$]	0.0257
wR_2 [$I > 2\sigma(I)$]	0.0714

D. IR and vibrational circular dichroism spectroscopy

Fourier transform infrared (FTIR) spectra were recorded on a Bruker Vertex 70 spectrometer with 2 cm^{-1} resolution. VCD spectra were recorded with the auxiliary Bruker PMA 50 module. KBr pellets were prepared with a mixture of KBr:L-His$^+$5NU$^-$ in a ratio of about 100:1. All VCD spectra were obtained during 1 h averaging time with 4 cm^{-1} resolution and the photoelastic modulator (PEM) at the center frequency of 1663 cm^{-1}.

III. THEORETICAL METHODS

A. Calculation of microscopic optical properties

The static α and β tensor components, used to calculate the macroscopic nonlinear optical properties, were computed with time-dependent density functional theory (TD-DFT) using the 6-311++G** basis set and the X3LYP extended exchange functional of Xu and Goddard III.[24] This functional is a combination of Slater, Becke,[25,26] and Perdew and Wang[27] exchange functionals plus Hartree-Fock exchange, with the correlation functional of Lee, Yang, and Parr.[28] The calculations were performed with the FIREFLY QC package,[29] which is partially based on the GAMESS (US) source code.[30] The microscopic unit considered was an interacting cation-anion pair with the ions' relative positions and geometries as in the crystal. The optical properties of the neutral molecules, as well as those of the individual ions, were also computed.

B. Calculation of macroscopic nonlinear optical properties

Since the intermolecular interactions are weak compared to the intramolecular chemical bonds, as is the case in most organic molecular crystals, the oriented gas model[31] is used to relate the macroscopic second-order susceptibility tensor d_{IJK} to the molecular quadratic hyperpolarizability tensor β_{ijk}. In this model, molecular hyperpolarizabilities are assumed to be additive and the crystalline susceptibilities are obtained by performing a tensor sum of the microscopic hyperpolarizabilities of the molecules that constitute the unit cell:

$$d_{IJK}(-\omega;\omega_1,\omega_2) = \frac{N}{V} f_I(\omega) f_J(\omega_1) f_K(\omega_2) b_{IJK},$$

$$b_{IJK} = \frac{1}{N_g} \sum_s \sum_{ijk} \cos\theta_{Ii}^{(s)} \cos\theta_{Jj}^{(s)} \cos\theta_{Kk}^{(s)} \times \beta_{ijk}^{(s)}(-\omega;\omega_1,\omega_2), \quad (1)$$

where I, J, and K are the crystal axes, N_g is the number of equivalent positions in the unit cell of volume V that has N molecules, $f_I(\omega)$ are local field factors appropriate for the crystal axis I, and the cosine product terms represent the rotation from the molecular reference frame onto the crystal frame. The equivalent positions are labeled by the index s. The local field factors are essentially a correction for the difference between an applied field that would be experienced by the molecule in free space and the local field detected in a material. According to Hamada,[32] the oriented-gas approximation may be meaningless if it is used without this correction.

We calculated the nonlinear optical properties of L-His$^+$5NU$^-$ using the methodology described by Silva *et al.*[33] We computed the unit cell nonlinearity per molecule, b_{IJK}, using the values of the microscopic quadratic polarizability β tensor components and taking into account the crystal symmetry of the material. The macroscopic NLO coefficients, d_{IJK}, were obtained using Eq. (1) with the Lorentz-Lorentz (L-L) (Ref. 34) or the Wortmann and Bishop (W-B) (Ref. 35) local field factors. The local field factors were calculated using the average linear polarizability of the unit cell per molecule, a_{II}.

C. Theory of vibrational circular dichroism

Vibrational circular dichroism is the differential absorption of left- and right-handed circularly polarized infrared light:

$$\Delta\varepsilon(\omega) = \varepsilon_{LCP}(\omega) - \varepsilon_{RCP}(\omega). \quad (2)$$

The magnitude of $\Delta\varepsilon(\omega)$ is proportional to the rotational strength of the associated infrared transition and requires the determination of the electric ($\vec{\mu}_{el}$) and magnetic ($\vec{\mu}_{mag}$) transition-dipole moments:

$$R = \mathrm{Im}\{\langle\Psi_i|\vec{\mu}_{\mathrm{el}}|\Psi_f\rangle \cdot \langle\Psi_f|\vec{\mu}_{\mathrm{mag}}|\Psi_i\rangle\}, \quad (3)$$

where $|\Psi_i\rangle$ and $|\Psi_f\rangle$ are the total wave functions for the initial and final states.[36] The calculation of the magnetic contribution to the rotational strength requires non-Born-Oppenheimer (BO) terms, since for a vibrational transition the contribution of the electronic part of $\vec{\mu}_{mag}$ is zero in the BO approximation. However, by means of perturbation theory, it can be shown that when a molecule is in an electronic state $|\psi_0\rangle$, the magnetic transition-dipole moment of a transition between the $\nu = 0$ and $\nu = 1$ levels of a vibrational mode is given to first order by[37,38]

$$\langle\Psi_f|\vec{\mu}_{\mathrm{mag}}|\Psi_i\rangle = \langle\chi_{\nu=0}| \sum_{n\neq 0} \frac{\langle\psi_0|\vec{\mu}^e_{\mathrm{mag}}|\psi_n\rangle}{E_n - E_0} (\langle\psi_n|T_{\mathrm{nucl}}|\psi_0\rangle - \langle\psi_0|T_{\mathrm{nucl}}|\psi_n\rangle)|\chi_{\nu=1}\rangle, \quad (4)$$

where $|\chi_{\nu=0}\rangle$ and $|\chi_{\nu=1}\rangle$ are the nuclear wave functions of the $\nu = 0$ and $\nu = 1$ states in the electronic state $|\psi_0\rangle$, and T_{nucl} is the nuclear kinetic energy operator. $|\psi_0\rangle$ and $|\psi_n\rangle$ are the electronic wave functions for the ground state and the nth electronically excited state, with energies E_0 and E_n, respectively.

VCD signals thus only arise if there is vibronically induced mixing of the BO wave functions associated with electronically excited states and the electronic ground state.[37] The sum-over-states expression given in Eq. (4) can under certain assumptions be contracted to a magnetic field derivative expression.[38] However, this approximation breaks down in case there are low-lying electronically excited states, and moreover do not provide a simple picture of the role played by the individual electronically excited states. We therefore performed, in addition to standard density-functional calculations to simulate the ground-state VCD spectra, TD-DFT calculations to obtain the excitation energies and the electronic magnetic transition-dipole moments between ground and excited states. In this manner, we can estimate the contribution of the low-lying excited-states to the VCD intensities by determining the coefficients $\langle\psi_0|\vec{\mu}^e_{\mathrm{mag}}|\psi_n\rangle/(E_n - E_0)$ in Eq. (4). All calculations were performed with GAUSSIAN 09 (Ref. 39) using the X3LYP extended exchange functional and the 6-311++G** basis set.

IV. RESULTS AND DISCUSSION

A. Crystal structure

The crystal structure of L-His$^+$5NU$^-$ (see Fig. 1) belongs to the monoclinic system with the noncentrossymmetric and chiral space group $P2_1$. Besides this structure, there are only two reported structures containing the 5-nitrouracilate (5NU$^-$) anion.[40,41] Figure 1 shows the conformation of the cation and anion in the salt. Of the two sites available for deprotonation in the heterocyclic ring of the 5-nitrouracil molecule (N1 and N3), deprotonation occurs at the more acidic N1.[42] Our calculations show that this causes a redistribution of π-electron density in the 5NU$^-$ anion that may be responsible for the increase in the molecular first hyperpolarizability of the anion compared with the neutral molecule. The pyrimidine ring is almost planar and the nitro group is rotated 4.2(1)° out of the plane of the uracil fragment. The L-histidinium cation occurs in the zwitterionic form, with protonated and positively charged α-amino and imidazolium groups and a deprotonated and negatively charged α-carboxylate group. The side chain of the cation adopts an

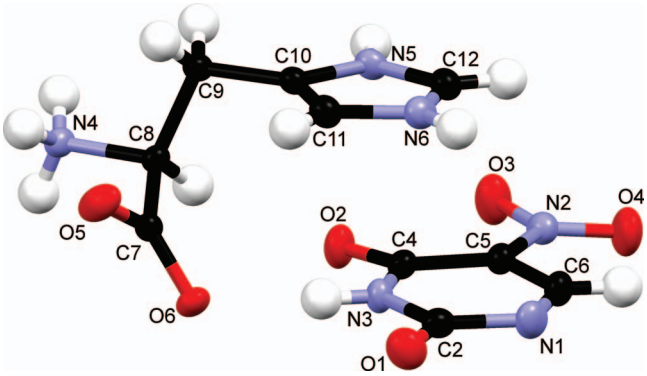

FIG. 1. Asymmetric unit of L-His$^+$5NU$^-$. The displacement ellipsoids are drawn at the 50% probability level (Mercury 2.4 (Ref. 43)).

open conformation II(t),[44] with torsion angles ϕ^1[N4-C8-C9-C10] = 179.0(1)° and ϕ^{21}[N5-C10-C9-C8] = 97.6(2)°.[45] As shown in Fig. 2, the amino group participates in three hydrogen bonds (see Table II), two of which have carboxylate oxygen atoms of another cation as acceptors, both delineating chains along [010] with a periodicity of five atoms, graph-set symbol C(5) according to Etters's graph-set theory.[46] In the other hydrogen bond involving the amino group, the acceptor is the O2 oxygen atom of the anion. The cations are also linked in chains along the a axis with descriptor C(7) via N−H···O hydrogen bonds involving the N$^+$−H group of the imidazolium ring and one oxygen atom of the carboxylate group of another cation. The cations are thus organized at $z = 0$ in infinite two-dimensional layers parallel to the plane (001). The 5NU$^-$ anions are anchored to the cationic sublattice by three hydrogen bonds (see Table II): the one already described; one involving the NH group of the cation and the N1 nitrogen atom of the anion, and one between the NH group of the anion and one carboxylate oxygen atom. There are no

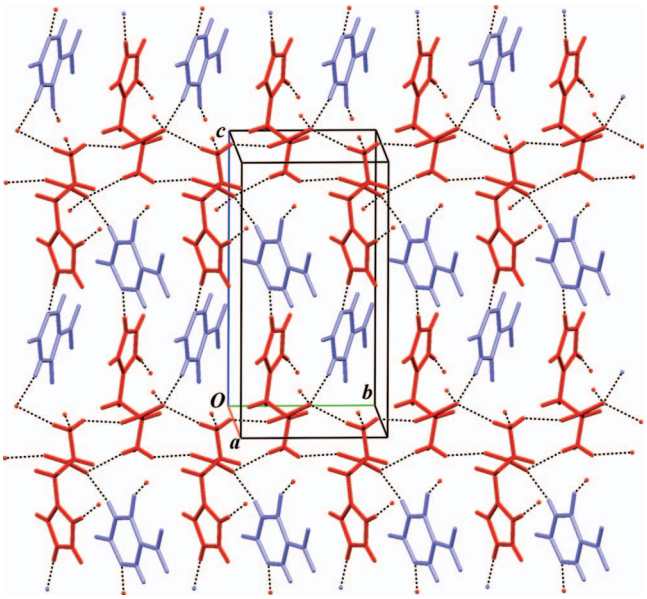

FIG. 2. Guest-host structure of L-His$^+$5NU$^-$. The anions (blue) are encapsulated between the cationic layers (red) in a polar herringbone motif along the b axis (Mercury 2.4 (Ref. 43)).

TABLE II. Hydrogen-bonding geometry (Å, degrees) of the L-His$^+$5NU$^-$ salt.

D-H···A	D-H	H···A	D···A	∠(D-H···A)
N1-H3···O6	0.86	2.03	2.880(2)	168.0
N4-H4A···O6^{i}	0.89	2.09	2.914(2)	153.9
N4-H4B···O5^{ii}	0.89	2.01	2.767(2)	141.7
N4-H4C···O2^{iii}	0.89	1.89	2.752(2)	164.1
N5-H5···O6^{iv}	0.86	2.00	2.852(2)	174.1
N6-H6A···N1^{v}	0.86	1.87	2.726(2)	178.1

Symmetry codes: *i*: $-x+2, y-1/2, -z$; *ii*: $-x+2, y+1/2, -z$; *iii*: $-x+1, y-1/2, -z$; *iv*: $x-1, y, z$; *v*: $-x+2, y-1/2, -z+1$.

hydrogen bonds between the anions. The L-His$^+$5NU$^-$ salt assumes a guest-host structure where the anions are encapsulated within the cationic layers in a polar herringbone motif along the b axis. The imidazolium and the pyrimidine rings are almost co-planar with a dihedral angle of 1.6(1)° between the least-square planes.

There are π-π stacking interactions between the imidazolium and the pyrimidine neighboring rings but these interactions are not symmetric on each side of a ring. There is a mildly strong π-π interaction between the pyrimidine ring (x, y, z) and the imidazolium ring (x, y, z), with a distance between the ring centroids d_{c-c} of 3.521(1) Å and a slipping angle β of 24.9° (β is the angle between the vector linking the ring centroids and the normal to the first ring). The other π-π contact between the pyrimidine ring (x, y, z) and the imidazolium ring (x, $y+1$, z) is weaker [d_{c-c} = 4.181(2) Å; β = 39.59°]. The imidazolium and pyrimidine rings are thus arranged in piles formed by the π-π interactions, with the distances between ring centroids alternating along the b axis between 3.521(1) and 4.181(2) Å.

B. Rietveld method for powder X-ray diffraction data

A Rietveld refinement[47] was performed with the Fullprof software[48] using the powder-diffraction data measured at room temperature. The overall parameters such as cell parameters, 2θ zero, scale factor, full-width at half-maximum and asymmetry parameter were allowed to refine in the range of 4 to 50°, with a final Bragg reliability factor of 12.3%. The excellent agreement between experimental and calculated patterns (see Fig. 3) confirms the high purity of the sample.

C. Nonlinear optical properties

The L-His$^+$5NU$^-$ crystal meets a series of features for a potentially highly efficient NLO material: (1) absence of an inversion center; (2) guest-host scheme with strong π-π interactions between the host (L-His$^+$) and the encapsulated guest (5NU$^-$); and (3) pink-colored crystals that show evidence for a charge-transfer (CT) complex since the starting reagents are white. TD-DFT calculations on the asymmetric unit of the crystal confirm this CT character: the lowest excited state is dominated by a HOMO−LUMO excitation in which the HOMO is localized on the 5NU$^-$ and the LUMO

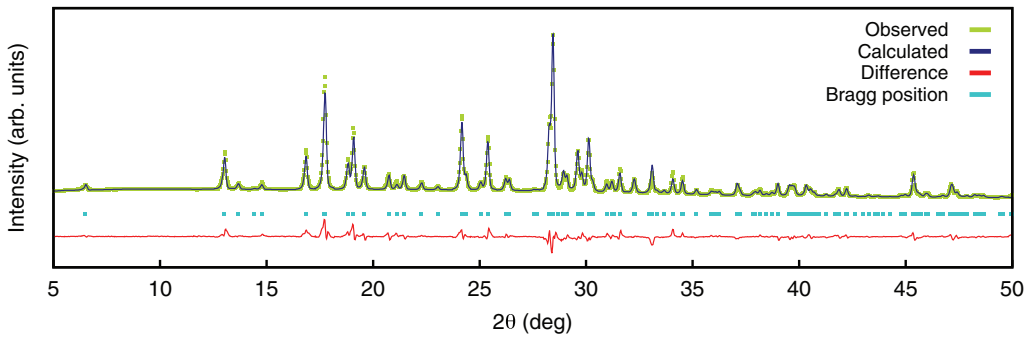

FIG. 3. Results from a least-squares fit using the Rietveld method: experimental powder diffraction pattern (green); simulated diffraction pattern using the Rietveld method (dark-blue); difference between the observed and calculated intensities (red), and corresponding Bragg positions (blue).

on the aromatic ring of the L-His$^+$. In Fig. 4 we show the difference density plots between ground and first excited state.

To determine the NLO response of the system we measured the SHG efficiency of the molecular crystal using a polycrystalline sample. A very high SHG efficiency of 10.5 times the standard KDP (or 3.5 × urea) was observed. Previously reported measurements on L-Histidinium salts show much lower SHG efficiencies.[49] In the following, a theoretical approach will be employed to quantify the strong second-order nonlinearities.

1. Low-lying electronic CT states

In standard time-dependent perturbation theory, the perturbed molecular ground state is expanded as a sum over all the electronic states of the unperturbed molecule. However, previously reported work describing the origin of the NLO response in a CT complex showed that the first hyperpolarizability β is largely determined by the lowest energy "through-space" CT excitation.[8] In this approximation, the low-lying electronically excited CT state is assumed to play the main role in describing the total optical response. Therefore, a two-level model[50] has been proposed to rationalize the first hyperpolarizability in systems where the dominant contributions to β originate from the ground state and a CT state:

$$\beta_{CT}(-2\omega;\omega,\omega) = \frac{3e^2}{2}\frac{\hbar\omega_{ge} f \Delta\mu_{ge}}{[(\hbar\omega_{ge})^2-(\hbar\omega)^2][(\hbar\omega_{ge})^2-(2\hbar\omega)^2]}, \quad (5)$$

where $\hbar\omega_{ge}$ is the CT excitation energy, f the oscillator strength for the CT excitation, and $\Delta\mu_{ge}$ the difference between the ground and excited state dipole moments. The latter term relates directly to an asymmetric change in the electronic distribution for the $|g\rangle \rightarrow |e\rangle$ transition, as observed in Fig. 4. The energy denominator is a crucial term since it can lead to a large enhancement of β if low-lying electronically excited states are present.

We used this model to calculate the β tensor of the interacting pair of ions which have a π-π interaction with a distance of 3.521(1) Å between ring centroids. From the TD-DFT calculations on the ion pair, we obtained the following results: $\Delta\mu_{ge}$ = 16.0 D, f = 0.005 and $\hbar\omega_{ge}$ = 2.39 eV (Table V). Substituting these values in Eq. (5) we obtain β_{CT} = 1856 a.u.

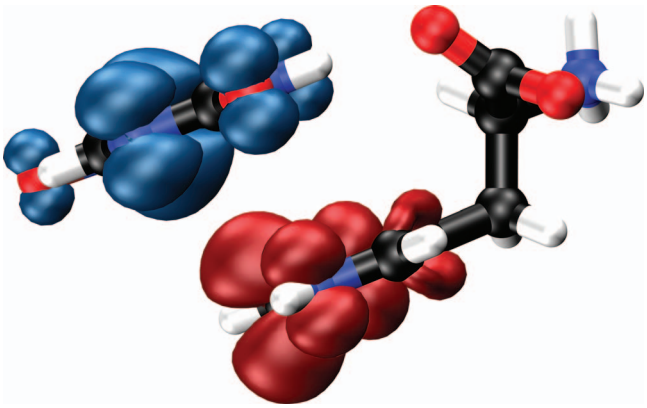

FIG. 4. Difference density plot (isovalue 0.004) between ground and excited state (S_1-S_0) of L-His$^+$5NU$^-$ obtained from a TD-DFT (X3LYP/6-311++G**) calculation. Blue indicates positive values and red negative values.

2. Microscopic and macroscopic nonlinear optical properties

The static α_{ij} and β_{ijk} tensor components were calculated according to the methods described in Sec. III A for the 5NU$^-$ anion, for the L-His$^+$ cation and for an interacting pair of ions. The calculations were performed in an orthogonalized crystalline reference frame where X is along the a axis and Y along the b axis. However, a better adapted molecular reference frame would facilitate the interpretation of the physical processes involved. For that reason, a transformation matrix was applied in order to have − in a molecular reference frame − the orthogonal y and z axis within a plane approximately parallel to the imidazolium and pyrimidine ring planes, perpendicular to the x axis. Since the ions assemble in the $P2_1$ space group, it is the angle of the common molecular plane with the crystalline polar two-fold axis that rules the macroscopic optical response. In the present case this angle is ∼60° which is very close to the optimal angle, 54.74° as deduced by Oudar and Zyss.[51] Importantly, Table III shows that the β tensor coefficients for the ionic pair are not the mere addition of the individual components. The most striking difference between the sum of the individual components and the value

TABLE III. Theoretical values of the full β tensor coefficients (a.u.) for the $5NU^-$ anion, for the L-His^+ cation and for an interacting pair of ions, in a molecular reference frame.

	$5NU^-$	L-His^+	$5NU^-$L-His^+
β_{xxx}	− 5.5	146.7	693.0
β_{yxx}	27.8	− 82.8	256.8
β_{zxx}	− 31.9	9.4	125.0
β_{xyy}	26.8	57.7	180.2
β_{yyy}	− 931.3	− 263.7	− 940.1
β_{zyy}	76.3	− 61.4	29.5
β_{xzz}	− 12.2	129.0	211.3
β_{yzz}	287.0	− 188.5	165.9
β_{zzz}	− 106.0	51.9	183.0
β_{xyz}	− 56.8	17.9	4.9

calculated for the interacting pair, happens for the β_{xxx} component. This suggests a significant charge transfer between adjacent ions, contributing to the quadratic polarizability.

The first hyperpolarizability β, being a fully symmetric third-rank tensor under Kleinmann symmetry,[52] can be decomposed into two tensorial components $\beta_{J=1}$ and $\beta_{J=3}$, called, respectively, the dipolar (vector) and the octupolar (septor) irreducible components:[6,53]

$$\beta = \beta_{J=1} \oplus \beta_{J=3} \tag{6}$$

From the vector and septor irreducible components, proper scalar invariants can be calculated. For molecules with no particular symmetry, the most general formulae, corresponding to class 1, must be used to calculate these invariants.[54] These quantities were calculated using the β components of the ionic pair (see Table III) yielding $\|\beta_{J=1}\| = 1248.1$ a.u. and $\|\beta_{J=3}\| = 1027.6$ a.u. The value for $\|\beta_{J=1}\|$, although calculated from static values, is comparable to that obtained from the much simpler two-level model ($\beta_{CT} = 1856$ a.u.).

Using the microscopic polarizabilities (α and β) of an interacting anion-cation pair, we calculated the susceptibility tensor $d_{IJK}(-2\omega; \omega, \omega)$ with the oriented gas model according to the methodology described in Sec. III B in its most general formulation. We did not make use of the expressions for systems with lower dimensionality (1D or 2D),[55] because of the ions' interaction. The crystal structure is monoclinic with space group $P2_1$, point group 2, so the only non-vanishing independent components of the susceptibility tensor allowed by this point group and by the Kleinman symmetry are d_{YXX}, d_{YYY}, d_{YZZ} and d_{XYZ}.[52,56] The results obtained with the L-L and the W-B local field corrections are presented in Table IV.

TABLE IV. Calculated susceptibility components (pm/V) for L-His^+5NU^- with L-L and W-B local field factors using as microscopic chromophoric unit a pair of interacting ions (L-His^+5NU^-). Figure of merit M_{IJK} (pm^2/V^2) for the phase-matchable components of d using W-B values.

	d_{YXX}	d_{YYY}	d_{YZZ}	d_{XYZ}
L-His^+5NU^- (L-L)	− 9.8	27.4	7.6	− 10.1
L-His^+5NU^- (W-B)	− 9.9	21.3	4.9	− 8.2
M_{IJK} (W-B)	21.1	...	5.5	15.0

As a benchmark, the d tensor for neutral 5-nitrouracil was also calculated using the same methodology: starting from the calculation of the microscopic properties, α and β, evolving to the calculation of the susceptibility tensor with the oriented gas model with the L-L and W-B local field corrections. The atomic coordinates used in the calculation were taken from the study by Rao an co-workers for the noncentrosymmetric orthorhombic polymorph, with space group $P2_12_12_1$.[57] The results for the only non-vanishing independent component, d_{XYZ}, were 19.6 pm/V (L-L) and 14.3 pm/V for the W-B local field factors, the latter value agreeing better with the experimental value of 8.7 pm/V.[58]

The predominance of d_{YYY} over the other susceptibility components can be explained by the previously mentioned stacking of the $5NU^-$ and L-His^+ ions along the b axis and the resulting CT interaction but, unfortunately, this component is not useful for birefringence phase-matching. Therefore, to predict the magnitude of the SHG signal, we calculated the birefringence phase-matching figure of merit:

$$M_{IJK} = \frac{d_{IJK}^2}{n_I n_J n_K} \tag{7}$$

for all the d components except d_{YYY} (see Table IV). The refractive indices n_I were obtained from the square root of the components of the dielectric constant tensor which was estimated according to the method described in Ref. 33.

Our measurements show that the SHG efficiency of L-His^+5NU^- is 3.5 times larger than that of urea, and since $M_{XYZ} = 1.5$ for urea standard (susceptibility of urea 2.3 pm/V; see Appendix I of Ref. 59), it is clear that the theory predicts the correct order of magnitude of the SHG response (see Table IV).

D. Vibrational circular dichroism

Section IV C has shown that a quantitative understanding of the nonlinear optical properties of the L-His^+5NU^- salt can be obtained from a two-state model. In the following we will show that the same model involving the same low-lying intermolecular charge transfer state can successfully reproduce the salient characteristics observed in the solid-state VCD spectrum of the compound. To this purpose we will compare VCD intensities of vibrational modes associated with the L-His^+ moiety in the L-His^+5NU^- salt and in the L-His^+Cl^- salt, the latter of which has no low-lying charge transfer state.

Figure 5 displays the experimental IR absorption and VCD spectra as obtained for L-His^+5NU^- and L-His^+Cl^-. Comparison of the intensities in the VCD spectra of the two salts shows strikingly larger intensities in the spectrum of the former. Indeed, a detailed comparison aided by the theoretically predicted spectra leads to the conclusion that the VCD intensities in L-His^+5NU^- are enhanced with respect to L-His^+Cl^- by an order of magnitude.

The theoretical framework of vibrational circular dichroism is well established[37,38] and the technique is nowadays routinely used to determine the absolute configuration of chiral molecules in solution and in solid samples.[60–64] In the past decade, an extension of the theory including molecular

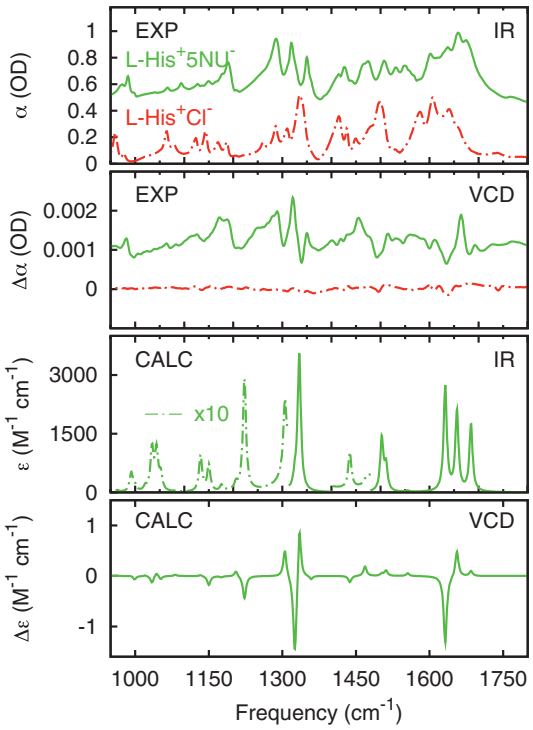

FIG. 5. Upper panels: Fourier-transform infrared (FTIR) and VCD spectra of L-His$^+$5NU$^-$ and L-His$^+$Cl$^-$ obtained with KBr pellet technique. Lower panels: Calculated IR and VCD spectra for L-His$^+$5NU$^-$ using DFT/X3LYP/6-311++G** level of theory. Some of the peaks are scaled for clear comparison with the experimental spectrum.

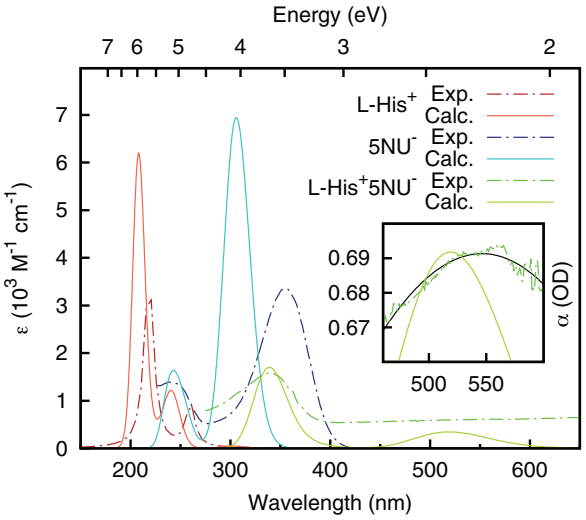

FIG. 6. Optical absorption spectra of L-His$^+$ (dashed-red), obtained with an acidic H_2O solution; 5NU$^-$ (blue), obtained from a basic H_2O solution; and the salt: L-His$^+$5NU$^-$, obtained with a 1 mm thin-film deposited in a 1 mm thick CaF_2 window. Calculated spectra were obtained at the TD-DFT/X3LYP/6-311++G** level of theory. Inset: enhanced range of the experimental spectrum of the thin-film of the salt to elucidate the presence of the band at 550 nm. Due to low intensity of the bands of the ionic salt, the extinction coefficients for the chromophores are scaled in intensity for clear comparison.

systems with low-lying electronic excited states has been described by Nafie.[65] This approach takes into account that vibronically induced mixing of the electronic wave functions with the ground state can lead to strongly enhanced VCD intensities. Recent work has demonstrated that it is possible to achieve up to one order of magnitude enhancement of the VCD signals in organic compounds by manipulation of the excited state manifold.[18] The present experiment shows for the first time that large intensity-enhanced VCD signatures can also be observed in a molecular crystal.

We find good agreement between observed and simulated VCD spectra (see Fig. 5). The majority of the peaks in the experimental spectrum can be assigned in the calculated spectrum with the correct sign and relative intensities.

In Sec. III C it has been discussed that one has to perform a summation over all excited states to obtain the magnetic term for the rotational strength (Eq. (4)). However, here we will show that in the present case a good estimate of the VCD signal intensities can be obtained by means of the two-level model used above to describe the NLO susceptibility.

In Fig. 6 we show the optical absorption spectra of the salt and its separate building blocks. For comparison with the level of theory implemented in the analysis, we also simulated UV-Vis spectra from the TD-DFT calculations. The agreement between experiment and theory is good. Figure 6 shows that upon formation of the salt, the electronic structure is altered as evidenced by the low-energy band observed around 550 nm (see inset Figure 6). In Table V we report the excitation energies and electronic magnetic transition-dipole moments for the lowest five electronically excited states in the salt and its building blocks.

The experimental VCD spectra give clear evidence for enhancement of VCD intensities in L-His$^+$5NU$^-$. A first theoretical estimate of the enhancement factor can be obtained from the coefficients $\langle\psi_0|\vec{\mu}^e_{\rm mag}|\psi_n\rangle/(E_n - E_0)$ in Eq. (4). To this purpose, we use the results obtained from the TD-DFT calculations, and consider only the first electronically excited state. From this approach we obtain an amplification factor of approximately 3, which is in good agreement with the observed enhancement of a factor of

TABLE V. Results of a TD-DFT//X3LYP/6-311++G** calculation on the salt and the individual building blocks for the five lowest excited states.

	Excitation	ΔE_{H-L} (eV)	$\langle\psi_0\|\vec{\mu}^e_{\rm mag}\|\psi_n\rangle$ (a.u.)	$\langle\psi_0\|\vec{\mu}^e_{\rm mag}\|\psi_n\rangle/(E_n - E_0)$
L-His$^+$	1	4.12	0.161	3.907×10^{-2}
	2	5.13	0.348	6.783×10^{-2}
	3	5.25	0.144	2.742×10^{-2}
	4	5.44	0.459	8.437×10^{-2}
	5	5.53	0.042	7.576×10^{-3}
5NU$^-$	1	3.67	0.519	1.414×10^{-1}
	2	3.98	0.449	1.128×10^{-1}
	3	4.02	0.572	1.423×10^{-1}
	4	4.29	0.608	1.417×10^{-1}
	5	4.60	0.567	1.233×10^{-1}
L-His$^+$5NU$^-$	1	2.39	0.249	1.046×10^{-1}
	2	2.91	0.019	6.500×10^{-3}
	3	3.22	0.118	3.660×10^{-2}
	4	3.26	0.050	1.530×10^{-2}
	5	3.38	0.161	4.760×10^{-2}

2−10 observed for the VCD intensities in the experimental spectrum of L-His$^+$5NU$^-$.

It is important to note that the contribution of the higher-lying excited states to the amplification is reduced by almost two orders of magnitude compared to that of the first excited state, which supports our two-level approximation. An estimate for the magnitude of the optical response can therefore be given through an analysis of the nature and characteristics of the excited state manifold. Here, the auxiliary low-lying electronically excited states generated through 5NU$^-$ have a striking influence in the VCD signals intensities. Nonetheless, it is interesting to note that, although not chiral, 5NU$^-$ also exhibits vibrational modes that have large VCD intensities, which must be caused by transfer of chirality from L-His$^+$ to 5NU$^-$.

V. CONCLUSIONS

In the present study, we have employed a two-state model to quantify the second-harmonic generation efficiency and vibrational circular dichroism spectral features of a new chiral organic material with enhanced NLO properties. Both optical responses are strongly amplified by the presence of a low-lying electronically excited charge-transfer state. The theoretical approach used here was shown to be successful in predicting the order of magnitude of the amplified linear and nonlinear optical responses. This approach should also be applicable to other nonlinear organic crystals, and thus might be valuable for predicting their nonlinear optical response and potential usefulness for nonlinear optical devices.

ACKNOWLEDGMENTS

We thank Ana Matos Beja, João Domingos, and Adriana Huerta-Viga for the technical support. This work was supported by the Fundo Europeu de Desenvolvimento Regional QREN-Compete through project PTDC/FIS/103587/2008 and PEst-C/FIS/UI0036/2011 Fundação para a Ciência e Tecnologia (FCT). S.R.D. and P.S.P.S. also acknowledge the fellowships SFRH/BD/48295/2008 and SFRH/BD/38387/2008 of FCT.

[1] *Nonlinear Optical Properties of Organic Molecules and Crystals*, edited by D. S. Chemla and J. Zyss (Academic, Oxford, 1987), Vol. 1.
[2] *Molecular Nonlinear Optics. Materials, Physics, and Devices*, edited by J. Zyss (Academic, Boston, MA, 1994).
[3] S. R. Marder, J. W. Perry, and W. P. Schaefer, Science **245**, 626 (1989).
[4] P. G. Lacroix, R. Clément, K. Nakatani, J. Zyss, and I. Ledoux, Science **263**, 658 (1994).
[5] J. Zyss, Abstracts of Papers of the American Chemical Society **21**, 33-PMSE (1991).
[6] J. Zyss, J. Chem. Phys. **98**, 6583 (1993).
[7] F. Meyers, S. R. Marder, B. M. Pierce, and J. L. Brédas, J. Am. Chem. Soc. **116**, 10703 (1994).
[8] S. DiBella, I. Fragala, M. A. Ratner, and T. J. Marks, J. Am. Chem. Soc. **115**, 682 (1993).
[9] P. G. Lacroix, I. I. Padilla-Martínez, H. L. Sandoval, and K. Nakatani, New J. Chem. **28**, 542 (2004).
[10] J. Zyss, I. Ledoux, S. Volkov, V. Chernyak, S. Mukamel, G. P. Bartholomew, and G. C. Bazan, J. Am. Chem. Soc. **122**, 11956 (2000).
[11] G. P. Bartholomew, I. Ledoux, S. Mukamel, G. C. Bazan, and J. Zyss, J. Am. Chem. Soc. **124**, 13480 (2002).
[12] T. Toury, J. Zyss, V. Chernyak, and S. Mukamel, J. Phys. Chem. A **105**, 5692 (2001).
[13] G. R. Meredith, *Nonlinear Optical Properties of Organic and Polymeric Materials* (American Chemical Society, Washington, DC, 1983), p. 27.
[14] C. Serbutoviez, J.-F. Nicoud, J. Fisher, I. Ledoux, and J. Zyss, Chem. Mater. **6**, 1358 (1994).
[15] S. Follonier, M. Fierz, I. Biaggio, U. Meier, C. Bosshard, and P. Günter, J. Opt. Soc. Am. B **19**, 1990 (2002).
[16] J. Zyss, J. Pécaut, J. P. Levy, and R. Masse, Acta Cryst. B **49**, 334 (1993).
[17] J. Zyss, R. Masse, M. Bagieu-Beucher, and J.-P. Lévy, Adv. Mater. **5**, 120 (1993).
[18] S. R. Domingos, M. R. Panman, B. H. Bakker, F. Hartl, W. J. Buma, and S. Woutersen, Chem. Commun. **48**, 353 (2012).
[19] Bruker, *SMART and SAINT* (Bruker AXS Inc., Madison, Wisconsin, USA, 2003).
[20] G. Sheldrick, SADABS, University of Göttingen, Germany, 2003.
[21] G. M. Sheldrick, Acta Crystallog., Sec. A **64**, 122 (2008).
[22] S. K. Kurtz and T. T. Perry, J. Appl. Phys. **39**, 3798 (1968).
[23] M. H. Garcia, J. C. Rodrigues, A. R. Dias, M. F. M. Piedade, M. T. Duarte, M. P. Robalo, and N. Lopes, J. Organomet. Chem. **632**, 133 (2001).
[24] X. Xu and W. A. Goddard III, Proc. Natl. Acad. Sci. U.S.A. **101**, 2673 (2004).
[25] A. D. Becke, Phys. Rev. A **38**, 3098 (1988).
[26] A. D. Becke, J. Chem. Phys. **98**, 5648 (1993).
[27] J. P. Perdew and Y. Wang, Phys. Rev. B **45**, 13244 (1992).
[28] C. Lee, W. Yang, and R. G. Parr, Phys. Rev. B **37**, 785 (1988).
[29] A. A. Granovsky, FIREFLY, version 7.1.G, 2009, see http://www.classic.chem.msu.su/gran/gamess/index.html, 2009.
[30] M. W. Schmidt, K. K. Baldridge, J. A. Boatz, S. T. Elbert, M. S. Gordon, J. H. Jensen, S. Koseki, N. Matsunaga, K. A. Nguyen, S. Su, T. L. Windus, M. Dupuis, and J. A. Montgomery, J. Comput. Chem. **14**, 1347 (1993).
[31] D. S. Chemla, J. L. Oudar, and J. Jerphagnon, Phys. Rev. B **12**, 4534 (1975).
[32] T. Hamada, J. Phys. Chem. **100**, 8777 (1996).
[33] P. S. P. Silva, C. Cardoso, M. R. Silva, J. A. Paixão, A. M. Beja, M. H. Garcia, and N. Lopes, J. Phys. Chem. A **114**, 2607 (2010).
[34] J. Schwinger, L. DeRaad, Jr., K. A. Milton, and W. Y. Tsai, *Classical Electrodynamics* (Perseus Books, 1998).
[35] R. Wortmann and D. M. Bishop, J. Chem. Phys. **108**, 1001 (1998).
[36] D. J. Caldwell and H. Eyring, *The Theory of Optical Activity* (Wiley-Interscience, New York, 1971).
[37] L. A. Nafie and T. B. Freedman, J. Chem. Phys. **78**, 7108 (1983).
[38] P. J. Stephens, J. Phys. Chem. **89**, 748 (1985).
[39] M. J. Frisch, G. W. Trucks, H. B. Schlegel *et al.*, GAUSSIAN 09, Revision C.02, Gaussian, Inc., Wallingford, CT, 2009.
[40] P. S. P. Silva, S. R. Domingos, M. R. Silva, J. A. Paixão, and A. M. Beja, Acta Crystallogr. Sect. E **64**, o1082 (2008).
[41] G. Portalone, Acta Crystallogr. Sect. C **66**, o295 (2010).
[42] G. Portalone and M. Colapietro, Acta Crystallogr. Sect. C, **63**, o650 (2007).
[43] C. F. Macrae, P. R. Edgington, P. McCabe, E. Pidcock, G. P. Shields, R. Taylor, M. Towler, and J. van de Streek, J. Appl. Cryst. **39**, 453 (2006).
[44] J. A. Krause, P. W. Baures, and D. S. Eggleston, Acta Crystallogr. Sect. B **47**, 506 (1991).
[45] IUPAC-IUB Commission on biochemical nomenclature, J. Mol. Biol. **52**, 1 (1970).
[46] M. C. Etter, Acc. Chem. Res. **23**, 120 (1990).
[47] *The Rietveld Method*, edited by R. A. Young (University Press, Oxford, 1993), Vol. 1.
[48] J. Rodriguez-Carvajal, Physica B **192**, 55 (1993).
[49] S. Aruna, G. Bhagavannarayana, and P. Sagayaraij, J. Cryst. Growth **304**, 184 (2007).
[50] J. L. Oudar and D. S. Chemla, J. Chem. Phys. **66**, 2664 (1977).
[51] J. L. Oudar and J. Zyss, Phys. Rev. A **26**, 2016 (1982).
[52] D. A. Kleinman, Phys. Rev. **126**, 1977 (1962).
[53] J. Jerphagnon, Phys. Rev. B **2**, 1091 (1970).
[54] J. Jerphagnon, D. Chemla, and R. Bonneville, Adv. Phys. **27**, 609 (1978).
[55] J. Zyss and J. L. Oudar, Phys. Rev. A **26**, 2028 (1982).
[56] R. W. Boyd, *Nonlinear Optics*, 3rd ed. (Academic, Burlington, MA, 2008).
[57] R. S. Gopalan, G. U. Kulkarni, and C. N. R. Rao, ChemPhysChem, **1**, 127 (2000).
[58] G. Puccetti, A. Perigaud, J. Badan, I. Ledoux, and J. Zyss, J. Opt. Soc. Am. B **10**, 733 (1993).
[59] *Nonlinear Optical Properties of Organic Molecules and Crystals*, edited by D. S. Chemla and J. Zyss (Academic, Orlando, FL, 1987), Vol. 2.
[60] T. B. Freedman, X. Cao, R. K. Dukor, and L. A. Nafie, Chirality **15**, 743 (2003).

[61]C. Merten, M. Amkreutz, and A. Hartwig, Phys. Chem. Chem. Phys. **12**, 11635 (2010).
[62]E. Schwartz, S. R. Domingos, A. Vdovin, M. Koepf, W. J. Buma, J. J. L. M. Cornelissen, A. E. Rowan, R. J. M. Nolte, and S. Woutersen, Macromolecules **43**, 7931 (2010).
[63]P. J. Stephens, F. J. Devlin, and J.-J. Pan, Chirality **20**, 643 (2008).
[64]V. P. Nicu, E. Debie, W. Herrebout, B. Van der Veken, P. Bultinck, and E. J. Baerends, Chirality **21**, E287 (2009).
[65]L. A. Nafie, J. Phys. Chem. A **108**, 7222 (2004).